PET of c-Met in Cancer with ^{64}Cu-Labeled Hepatocyte Growth Factor

Haiming Luo[1], Hao Hong[1], Michael R. Slater[2], Stephen A. Graves[3], Sixiang Shi[4], Yunan Yang[1], Robert J. Nickles[4], Frank Fan[2], and Weibo Cai[1,3–5]

[1]Department of Radiology, University of Wisconsin–Madison, Madison, Wisconsin; [2]Promega Corp., Madison, Wisconsin; [3]Department of Medical Physics, University of Wisconsin–Madison, Madison, Wisconsin; [4]Materials Science Program, University of Wisconsin–Madison, Madison, Wisconsin; and [5]University of Wisconsin Carbone Cancer Center, Madison, Wisconsin

The hepatocyte growth factor (HGF) and its receptor, c-Met, are actively involved in tumor progression and metastasis and are closely associated with a poor prognostic outcome for cancer patients. Thus, the development of PET agents that can assess c-Met expression would be extremely useful for diagnosing cancer and subsequently monitoring response to c-Met–targeted therapies. Here, we report the characterization of recombinant human HGF (rh-HGF) as a PET tracer for detection of c-Met expression in vivo. **Methods:** rh-HGF was expressed in human embryonic kidney 293 cells and purified by nickel-nitrilotriacetic acid affinity chromatography. The concentrated rh-HGF was conjugated to 2-*S*-(4-isothiocyanatobenzyl)-1,4,7-triazacyclononane-1,4,7-triacetic acid and labeled with ^{64}Cu. c-Met binding evaluation by flow cytometry was performed on both U87MG and MDA-MB-231 cell lines, which have a high level and a low level, respectively, of c-Met. PET imaging and biodistribution studies were performed on nude mice bearing U87MG and MDA-MB-231 xenografted tumors. **Results:** The rh-HGF expression yield was 150–200 μg of protein per 5×10^6 cells after a 48-h transfection, with purity of approximately 85%–90%. Flow cytometry examination confirmed that rh-HGF had a strong and specific capacity to bind to c-Met. After ^{64}Cu labeling, PET imaging revealed specific and prominent uptake of ^{64}Cu-NOTA-rh-HGF in c-Met–positive U87MG tumors (percentage injected dose per gram, 6.8 ± 1.8 at 9 h after injection) and significantly lower uptake in c-Met–negative MDA-MB-231 tumors (percentage injected dose per gram, 1.8 ± 0.6 at 9 h after injection). The fact that sonication-denatured rh-HGF had significantly lower uptake in U87MG tumors, along with histology analysis, confirmed the c-Met specificity of ^{64}Cu-NOTA-rh-HGF. **Conclusion:** This study provided initial evidence that ^{64}Cu-NOTA-rh-HGF visualizes c-Met expression in vivo, an application that may prove useful for c-Met–targeted cancer therapy.

Key Words: c-Met; hepatocyte growth factor (HGF); positron emission tomography (PET); ^{64}Cu; cancer

J Nucl Med 2015; 56:758–763
DOI: 10.2967/jnumed.115.154690

A tyrosine kinase receptor for hepatocyte growth factor (HGF) called c-Met is overexpressed or aberrantly activated in a variety of cancers, including renal, ovarian, lung, colorectal, breast, gastric, cervical, pancreatic, and esophageal cancer, as well as melanoma (*1,2*). The overexpression of c-Met from gene amplification or mutation in cancer results in aberrant activation of the c-Met axis, leading to proliferation, apoptosis inhibition, angiogenesis, and invasion of cancer cells (*3*). c-Met overexpression is also associated with poor clinical prognosis, elevated occurrence of metastasis, and increased drug resistance of cancer (*4,5*). Together, these characteristics suggest that c-Met is an active participant in cancer initiation and progression, and thus the assessment of c-Met expression in real time could potentially aid in diagnosis and in monitoring of response to therapy.

Numerous studies also suggest that c-Met is an attractive drug target in cancer therapy because blocking of c-Met can usually inhibit tumor growth and metastasis (*2,6*). Multiple clinical trials have adopted tyrosine kinase inhibitors and monoclonal antibodies against c-Met pathways as cancer therapeutic agents (*7–9*). Diagnostic methods of identifying the suitable patient population for c-Met–targeted therapy are fundamental to improve clinical outcome. The current patient selection standard is usually based on immunohistochemistry or fluorescent in situ hybridization. Although these methods can provide quantitative information about c-Met abundance, they are not applicable in two scenarios: reflecting c-Met expression fluctuation over time, and dealing with c-Met heterogeneity in different tumor sites. PET imaging can overcome these limitations because of its high sensitivity in the real-time detection of molecular events. Several radiolabeled antibodies against c-Met have already been used for in vivo tumor targeting. PRS-110, an Anticalin (Pieris Pharmaceuticals, Inc.) with monovalent specificity for c-Met, was labeled with ^{89}Zr (half-life, 78.4 h) for imaging U87MG glioblastoma. Moderate tumor accumulation (4 percentage injected dose per gram [%ID/g]) was obtained in that study (*10*). Other choices such as DN30 and onartuzumab have also been labeled with ^{89}Zr for imaging c-Met expression in vivo, with good tumor uptake (*11,12*). However, the prolonged circulation time and slow clearance can lead to low tumor-to-background ratio and limit their clinical applicability as diagnostic agents.

HGF, the only known ligand for c-Met, is usually secreted as an inactive polypeptide and cleaved by serine proteases into the bioactive format comprising a 69-kDa α chain and a 34-kDa β-chain linked by a disulfide bond (*9*). There were several earlier attempts to express biologically active recombinant human HGF (rh-HGF) in both *Escherichia coli* and insect cells (*13,14*). Although the biologic activity of rh-HGF produced from *E. coli* has been reported to be equivalent to its native form (*15*), the absence of the disulfide bond formation and lack of molecular glycosylation

Received Jan. 22, 2015; revision accepted Mar. 9, 2015.
For correspondence or reprints contact: Weibo Cai, Department of Radiology, University of Wisconsin–Madison, Room 7137, 1111 Highland Ave., Madison, WI 53705-2275.
E-mail: wcai@uwhealth.org.
Published online Apr. 3, 2015.

can potentially compromise its applicability in vivo. Furthermore, production of rh-HGF in *E. coli* inclusion bodies involves a refolding process (*15*), which is time-consuming and usually causes a low protein production yield. For similar reasons, insect cells are not ideal hosts for expressing human glycoproteins because of different glycosylation levels (*16*). To attain rh-HGF with an equivalent structure to the native form, expression in mammalian cells, including COS-1, rat hepatocytes, and Chinese hamster ovary cells, is preferred (*17–19*).

In this study, we used mammalian human embryonic kidney (HEK) 293 cells to express 10His-tagged rh-HGF. After attaining rh-HGF with high purity, we used PET imaging to investigate the in vivo distribution pattern and c-Met–targeting efficacy of ^{64}Cu-labeled rh-HGF (named ^{64}Cu-NOTA-rh-HGF). Two human cancer cell lines were selected, that is, U87MG glioblastoma with high c-Met expression and MDA-MB-231 breast cancer cells with low c-Met expression. Region-of-interest analysis of PET images was also performed to quantify uptake of ^{64}Cu-NOTA-rh-HGF in major tissues and organs. Histology evaluation was also provided to confirm that uptake of ^{64}Cu-NOTA-rh-HGF in tumors was relevant to c-Met expression.

MATERIALS AND METHODS

Plasmids and Cell Lines

The plasmid cytomegalovirus promoter (pCMV)–human HGF-10his (Sino Biologic Inc.) was used in the cloning and expression procedure. Large-scale plasmid DNA was extracted with an EZNA Plasmid Mini Kit II (Omega). The *E. coli* DH5α (Invitrogen) was used as a host for cloning of pCMV-human HGF-10his.

U87MG human glioblastoma and MDA-MB-231 human breast cancer lines were obtained from the American Type Culture Collection and cultured according to the supplier's instructions. All animal studies were conducted under a protocol approved by the University of Wisconsin Institutional Animal Care and Use Committee. U87MG and MDA-MB-231 tumor models were prepared using a method similar to one previously described (*20*).

Expression and Purification of rh-HGF

HEK293 cells (5×10^6) were seeded onto 150-cm^2 cell culture flasks, and transfection was performed with 46.9 μg of pCMV-human HGF-10his DNA using the FuGENE HD reagent (Promega) when cell density reached 70%, according to the manufacturer's protocol. After 2 d, the cells were collected via Cellstripper (Corning) and lysed by 1 × mammalian lysis buffer (Promega). Repeated freezing and thawing steps were performed on the cell suspension to release the recombinant proteins.

The rh-HGF encoded by pCMV carries 10 histidine residues at its C terminus. The nickel-nitrilotriacetic acid was balanced by binding buffer before the supernatant of lysed cells containing rh-HGF was added to the column, and the proteins associated with the resin were eluted by applying increasing concentrations of imidazole in the buffer. The details of the purification procedures have been previously published (*21*). The purity of rh-HGF was evaluated with 8% sodium dodecyl sulfate polyacrylamide gel electrophoresis (SDS-PAGE) gel under nonreducing conditions stained with Coomassie (Imperial Chemical Industries) brilliant blue R-250.

rh-HGF Conjugation and Radiolabeling

NOTA-rh-HGF was prepared using a method similar to one previously described (*20*). Briefly, NOTA conjugation was performed at pH 9.0 with the reaction ratio of 2-*S*-(4-isothiocyanatobenzyl)-1,4,7-triazacyclononane-1,4,7-triacetic acid:rh-HGF being 10:1 at room temperature for 1 h. PD-10 columns were used to purify NOTA-rh-HGF, with phosphate-buffered saline as the mobile phase. Similar reaction conditions were adopted for the conjugation of rh-HGF with *N*-hydroxy-succinimidyl-ester fluorescein (Thermo Scientific Pierce). ^{64}Cu labeling and purification followed the routine protocol described by our group previously (*20*). $^{64}CuCl_2$ (37 MBq) was diluted in 300 μL of 0.1 M sodium acetate buffer (pH 6.5) and added to 20 μg of NOTA-rh-HGF.

Flow Cytometry

The biologic activity of purified rh-HGF was evaluated by flow cytometry. Briefly, U87MG and MDA-MB-231 cells were incubated with a 20 μg/mL concentration of rh-HGF for 1 h. Subsequently, the cells were incubated with mouse antihuman HGF antibody (Thermo Scientific) for 4 h and with fluorescein isothiocyanate (FITC)–labeled goat antimouse secondary antibody for 1 h. For evaluation of the c-Met expression levels, U87MG and MDA-MB-231 cells were fixed by cold 4% paraformaldehyde before the 2-step incubation with rat antihuman c-Met antibody (eBioscience) at 4°C overnight and with Cy3 conjugated donkey antirat secondary antibody for 1 h.

The c-Met–binding specificity of rh-HGF to U87MG and MDA-MB-231 cells was further confirmed by incubation of cells with 50 nM FITC-rh-HGF or FITC-NOTA-rh-HGF for 30 min. Sonication-denatured FITC-dnrh-HGF was used as a control. All cells were washed and analyzed with a FACSCalibur 4-color analysis cytometer (Becton-Dickinson) with FlowJo analysis software (Three Star, Inc.)

PET Imaging and Biodistribution Studies

PET scanning, image reconstruction, and region-of-interest analysis of each PET scan were performed using an Inveon small-animal PET/CT scanner (Siemens Medical Solutions USA, Inc.) as described previously (*20*). Each tumor-bearing mouse was intravenously injected with 5–10 MBq of ^{64}Cu-NOTA-rh-HGF, and 5- to 10-min static PET scans were obtained at various time points after injection. The tracer uptake was calculated as %ID/g (mean ± SD; ≥3 mice per group).

The c-Met specificity of ^{64}Cu-NOTA-rh-HGF in vivo was evaluated using denaturing studies, in which each mouse of a group of 3 was injected with 5–10 MBq of sonication-denatured tracer, ^{64}Cu-NOTA-dnrh-HGF. Biodistribution studies were performed after the last PET scans at 24 h after injection to validate the PET data. The tumors, liver, and muscle were also frozen and cryosectioned for histologic analysis. Quantitative data were expressed as mean ± SD. Means were compared using the Student *t* test. *P* values of less than 0.05 were considered statistically significant.

Histology

After blocking with 10% donkey serum, frozen tissue slices of 5-μm thickness were incubated with rh-HGF (20 μg/mL) for 1 h at 4°C. After washing with phosphate-buffered saline, the slices were incubated with mouse antihuman HGF mAb for 4 h, followed by FITC-labeled goat antimouse IgG for 1 h. The tissue slices were also stained with rat antihuman c-Met antibody and Cy3-labeled donkey antirat IgG. All images were acquired with an Eclipse Ti confocal microscope (Nikon).

RESULTS

Expression and Purification of rh-HGF

To attain a high level of rh-HGF, we chose the human cytomegalovirus promoter because of its potent expression efficiency for a downstream gene. As shown in Figure 1A, under a human cytomegalovirus–driven constitutive promoter, the human HGF gene can be expressed in mammalian cells as a tagged protein with a C-terminal 10His tag, which can be used for further product purification. Transient transfections were performed using the mammalian cell line HEK293 and the procedures described above.

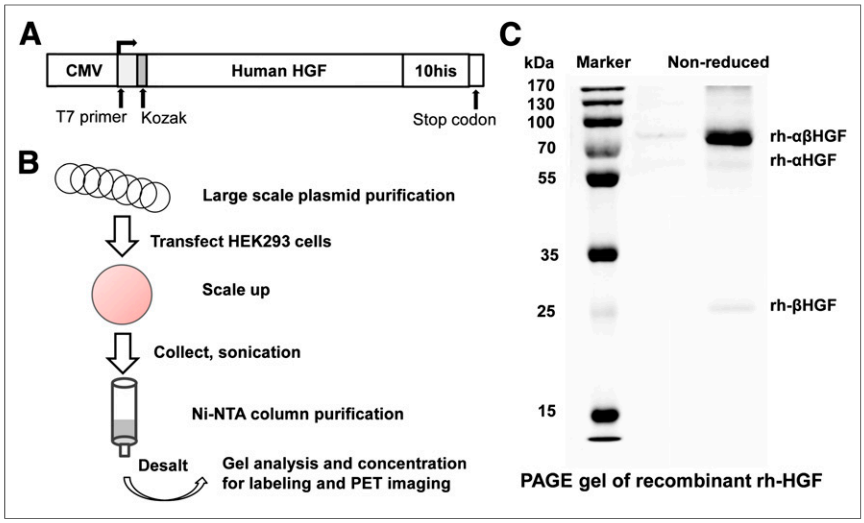

FIGURE 1. Expression and purification of rh-HGF. (A) Schematic representation of pCMV-human HGF construct. Functional elements of expression vector are pCMV (human cytomegalovirus immediate early I promoter/enhancer), T7 primer (T7 promoter priming site), Kozak (Kozak translation-initiation sequence and initiation codon [ATG] for proper initiation of translation), and human HGF-10his tag (human HGF protein fused to 10his tag). (B) Schematic representation of steps involved in expression of secreted proteins from stable mammalian cell lines. (C) SDS-PAGE (8%) analysis of purified rh-HGF transiently expressed in HEK293 cells. Molecular weight markers are shown on left. NTA = nitrilotriacetic acid.

After 2 d of incubation with FuGENE HD and recombinant plasmid, protein production yield was initially tested by SDS-PAGE. After high-yield protein production in the cells had been confirmed, large-scale purification was performed. After cell lysis, nickel-nitrilotriacetic acid resin was used to capture the 10His-tagged rh-HGF. The schematic workflow for rh-HGF protein expression and purification is illustrated in Figure 1B. There was one clear band at 90 kDa on SDS-PAGE under nonreducing conditions, which represented the bioactive rh-HGF, and its purity was approximately 85%–90%. Two weak bands at the molecular weight of 60 and 34 kDa were also shown on SDS-PAGE, corresponding to the α chain and β chain, respectively, of HGF (Fig. 1C).

Characterization of rh-HGF

FITC-conjugated antihuman HGF antibody was used to visualize rh-HGF binding to U87MG and MDA-MB-231 cells. Most of the U87MG cells showed high levels of cell surface–bound rh-HGF based on enhanced cellular fluorescence (Fig. 2A). To confirm the cellular expression level of c-Met, Cy3-labeled antic-Met antibody was used in U87MG and MDA-MB-231 cells. The flow cytometry results showed that the c-Met expression level of U87MG was significantly higher than that of MDA-MB-231 (Fig. 2B). Together, these results indicated that purified rh-HGF protein had high binding affinity to cellular c-Met. The binding level of rh-HGF to U87MG and MDA-MB-231 cells was in accordance with their c-Met expression levels.

To further confirm the cellular binding specificity of rh-HGF, c-Met–positive U87MG cells were incubated with 50 nM of FITC-conjugated rh-HGF, NOTA-rh-HGF, or sonication-denatured dnrh-HGF. Figure 2C shows that there were no observable differences in cellular uptake between FITC-rh-HGF and FITC-NOTA-rh-HGF, whereas the uptake of FITC-rh-HGF was significantly higher than that of FITC-dnrh-HGF. Together with the extremely low uptake of FITC-rh-HGF in MDA-MB-231, these results confirmed that NOTA conjugation did not compromise the binding affinity or specificity of rh-HGF for c-Met.

PET and Biodistribution Studies

Time points of 0.5, 3, 9, 15, and 24 h after injection were chosen for serial PET scans after intravenous injection of ^{64}Cu-NOTA-rh-HGF into tumor-bearing mice. The coronal slices that contained the tumors are shown in Figure 3, and the quantitative data obtained from region-of-interest analysis of PET results are shown in Figure 4. In U87MG tumor, which expresses a high level of c-Met, ^{64}Cu-NOTA-rh-HGF accumulated rapidly, was clearly visible in tumors at 0.5 h after injection, peaked at 9 h after injection, and remained stable over time (5.5 ± 2.0, 6.7 ± 1.5, 6.8 ± 1.8, 5.9 ± 1.4 and 5.4 ± 0.9 %ID/g at 0.5, 3, 9, 15, and 24 h, respectively, after injection [n = 4] [Fig. 4A]). Liver uptake (36.0 ± 0.3, 32.7 ± 4.5, 26.0 ± 3.0, 24.5 ± 4.3, and 21.3 ± 2.7 %ID/g at 0.5, 3, 9, 15, and 24 h, respectively, after injection) and kidney uptake (30.5 ± 1.0, 26.6 ± 1.3, 19.6 ± 1.0, 14.3 ± 1.1, and 10.0 ± 2.2 %ID/g at 0.5, 3, 9, 15, and 24 h, respectively, after injection [Fig. 4A]) were similar to those in c-Met–negative MDA-MB-231 tumor models. Uptake in most other organs was very low. On comparison, uptake of ^{64}Cu-NOTA-rh-HGF in MDA-MB-231 tumor was low (1.5 ± 2.0, 1.6 ± 0.5, 1.8 ± 0.6, 1.7 ± 0.6, and 1.6 ± 0.6 %ID/g at 0.5, 3, 9, 15, and 24 h, respectively, after injection [n = 3] [Fig. 4B]). These values were significantly lower than those of U87MG tumors at all time points ($P < 0.05$), indicating that c-Met targeting is the primary reason for the prominent uptake of ^{64}Cu-NOTA-rh-HGF in U87MG tumor.

^{64}Cu-NOTA-dnrh-HGF (which was sonication-denatured and hence did not bind to c-Met) had significantly lower U87MG tumor uptake than ^{64}Cu-NOTA-rh-HGF, with 1.0 ± 0.2, 1.2 ± 0.3, 1.4 ± 0.5, 1.6 ± 0.6, and 1.6 ± 0.3 %ID/g at 0.5, 3, 9, 15, and 24 h, respectively, after injection (n = 3; $P < 0.05$ at all time points) (Figs. 4C and 4D). Liver uptake (34.9 ± 1.6, 30.3 ± 1.8, 25.3 ± 0.5, 22.2 ± 0.7, and 19.9 ± 1.2 %ID/g at 0.5, 3, 9, 15, and 24 h, respectively, after injection [n = 3] [Fig. 4C]) and kidney uptake (30.7 ± 0.4, 25.5 ± 1.4, 19.6 ± 1.0, 16.3 ± 1.0, and 13.7 ± 1.0 % ID/g at 0.5, 3, 9, 15, and 24 h, respectively, after injection [n = 3] [Fig. 4C]) of ^{64}Cu-NOTA-dnrh-HGF were comparable to those of mice injected with ^{64}Cu-NOTA-rh-HGF, since both the liver and the kidneys are the expected clearance organs for a tracer of this size. Overall, tracer uptake was similar between ^{64}Cu-NOTA-rh-HGF and ^{64}Cu-NOTA-dnrh-HGF in all major organs except U87MG tumor (significantly higher in ^{64}Cu-NOTA-rh-HGF), further confirming the c-Met specificity of the tracer.

After the terminal PET scans at 24 h after injection, all mice were euthanized for biodistribution studies to validate quantitative tracer uptake values based on PET imaging data. The U87MG tumor uptake of ^{64}Cu-NOTA-rh-HGF was 5.9 ± 1.3 %ID/g at 24 h after injection, significantly higher than the uptake of ^{64}Cu-NOTA-dnrh-HGF in U87MG tumor (1.4 ± 0.4 %ID/g) and the uptake of ^{64}Cu-NOTA-rh-HGF in MDA-MB-231 tumor

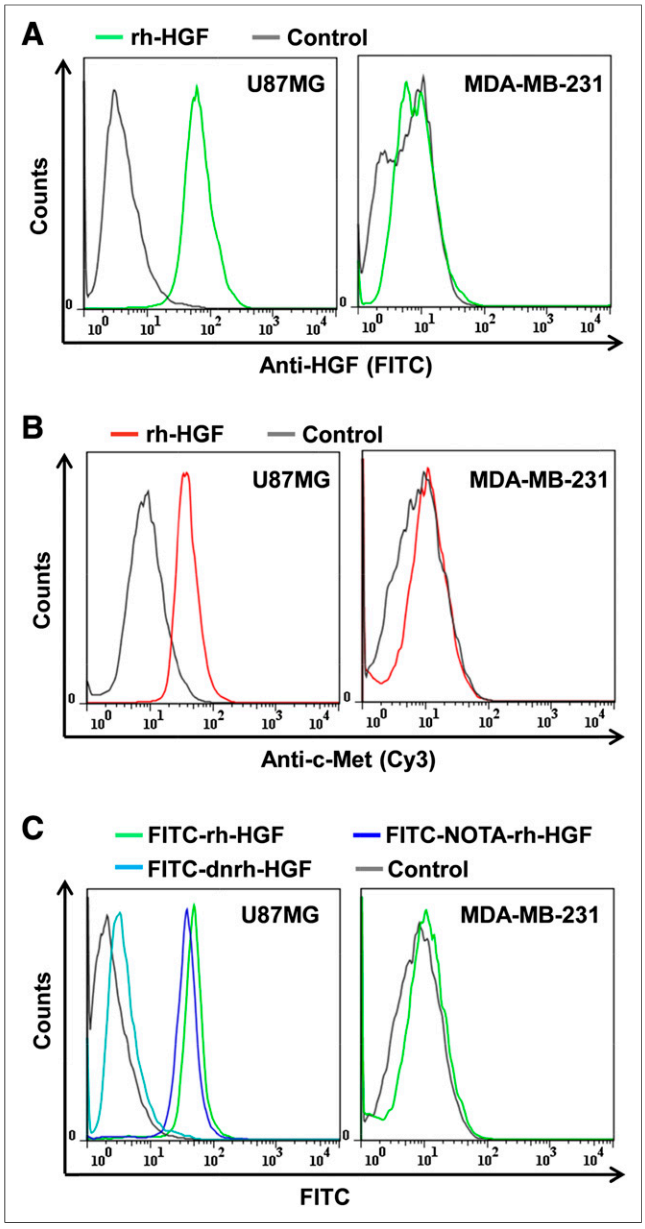

FIGURE 2. Evaluation of c-Met binding capability of rh-HGF by flow cytometry. (A) Assessment of rh-HGF binding to c-Met–positive U87MG and c-Met–negative MDA-MB-231 cells. rh-HGF was incubated with cells first, followed by mouse antihuman HGF antibody and FITC-conjugated goat antimouse IgG for flow cytometry analysis. (B) Assessment of c-Met expression level in U87MG and MDA-MB-231 cells by flow cytometry with rat antihuman c-Met antibody and Cy3-labeled donkey antirat IgG. (C) Flow cytometry analysis in U87MG and MDA-MB-231 cells confirmed specificity of rh-HGF and NOTA-rh-HGF for c-Met. dnrh-HGF does not bind to c-Met.

(0.7 ± 0.3 %ID/g) (Fig. 5). As a result, U87MG tumor uptake of ^{64}Cu-NOTA-rh-HGF was the highest and provided excellent tumor contrast, with a 13.5 ± 6.1 (n = 4) tumor-to-muscle ratio at 24 h after injection. Overall, quantification data obtained from the biodistribution studies were consistent with PET scan results, indicating that region-of-interest analysis of noninvasive PET scans truly reflected tracer distribution in vivo, as well as the c-Met specificity of ^{64}Cu-NOTA-rh-HGF.

Histology

On the basis of fluorescence staining of c-Met, c-Met expression was prominent on the U87MG tumor cells but absent on the MDA-MB-231 cells, and rh-HGF could target c-Met with high specificity (Fig. 6). c-Met staining of mouse liver and muscle gave a low signal, indicating that these tissues do not express a high level of c-Met. Thus, uptake of ^{64}Cu-NOTA-rh-HGF in liver was due mostly to hepatic clearance of the tracer rather than to c-Met binding. The fluorescence from FITC-rh-HGF provided an excellent overlay with c-Met in U87MG tumor but not in MDA-MB-231 tumor.

DISCUSSION

The HGF/c-Met signaling pathway has emerged as a promising therapeutic target for inhibiting tumor growth (*22*). Activation or upregulation of c-Met is a negative prognostic indicator for various carcinomas, multiple myeloma, and glioma (*9*). Several strategies to inhibit c-Met activation are currently under clinical evaluation, such as the use of tyrosine kinase inhibitors, monoclonal antibodies (against the receptor or ligand), and compounds against c-Met/HGF (*8,23*). To obtain a more accurate clinical outcome, suitable biomarkers are needed to noninvasively monitor and predict response to therapy. ^{18}F-labeled FDG and FLT for PET imaging (*24,25*) and gadolinium-labeled antic-Met antibody for MR imaging (*26*) have been investigated. However, as the only known ligand of c-Met, HGF has not been used for PET imaging to quantify c-Met abundance. Because HGF is a multifunctional growth factor involved in stimulation of hepatocyte proliferation, inhibition of apoptosis, and invasive growth of tumor cells (*27*),

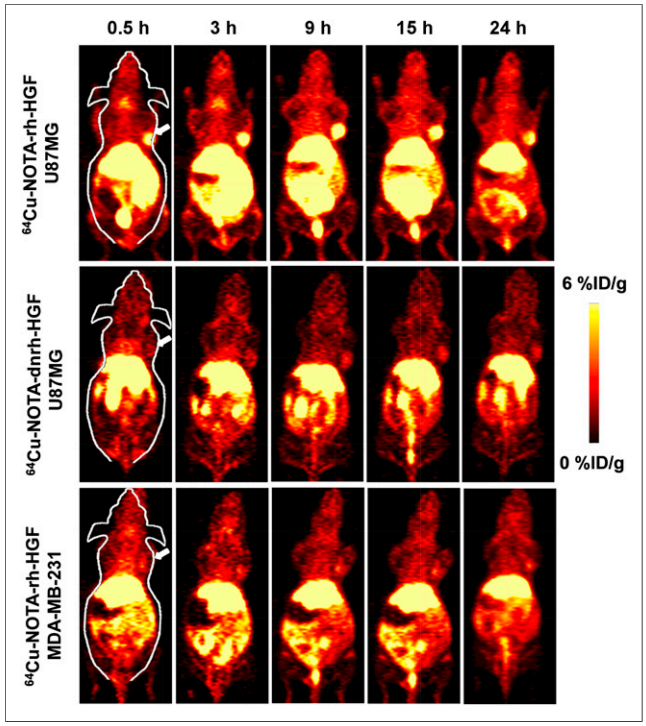

FIGURE 3. Small-animal PET imaging of c-Met expression in U87MG and MDA-MB-231 tumor–bearing mice. Serial coronal PET images at 0.5, 3, 9, 15, and 24 h after injection of ^{64}Cu-NOTA-rh-HGF or ^{64}Cu-NOTA-dnrh-HGF are shown, and tumors are indicated by arrows.

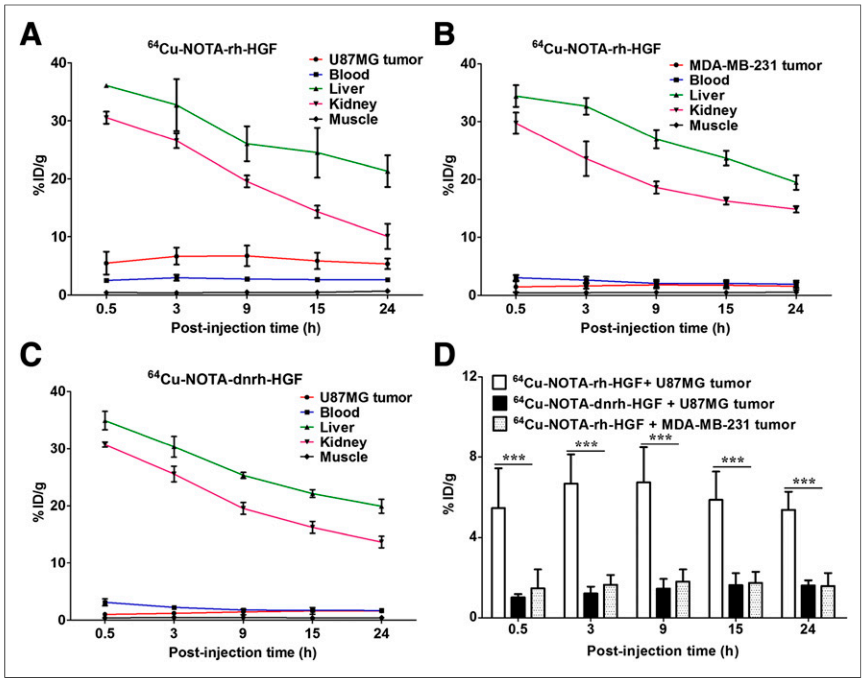

FIGURE 4. Quantitative analysis of PET data. (A) Time–activity curves of U87MG tumor, blood, liver, kidney, and muscle on intravenous injection of ^{64}Cu-NOTA-rh-HGF. (B) Time–activity curves of MDA-MB-231 tumor, blood, liver, kidney, and muscle on intravenous injection of ^{64}Cu-NOTA-rh-HGF. (C) Time–activity curves of U87MG tumor, blood, liver, kidney, and muscle on intravenous injection of ^{64}Cu-NOTA-dnrh-HGF. (D) Comparison of tumor uptake in all 3 groups ($n \geq 3$).

rh-HGF has been used in a clinical trial for treatment of fulminant hepatic failure or late-onset hepatic failure (*28*). Developing a HGF-based PET tracer for imaging of c-Met expression in cancer patients may significantly facilitate patient stratification in clinical trials, as well as provide for surveillance of the efficacy of c-Met-targeted therapies.

To avoid proteolytic digestion and complexity in downstream processes, including disulfide bonds and unique glycosylation patterns, the production of HGF requires eukaryotic or even mammalian expression systems to achieve high yields of functional active protein (*29*). A simple but robust protocol was established in this study using pCMV standard vector with 10His tag and transient expression in HEK293 cells to produce rh-HGF with high purity and quantity. After purification, 150–200 μg of rh-HGF per 150-cm^2 flask could be obtained after a 48-h transfection. SDS-PAGE gel analysis showed a major constituent with a molecular weight of 90 kDa, standing for purified rh-HGF. Two weak bands about 60 and 30 kDa were also seen on SDS-PAGE, as was consist with the reported result for rh-HGF in the Chinese hamster ovary expression system since there is an equilibrium between rh-HGF and its α/β chain (*19*). 10His tag was used to simplify the production and characterization of rh-HGF and did not affect the function of rh-HGF, as confirmed by the potent and specific capacity of rh-HGF to bind to c-Met based on flow cytometry (Fig. 2). The 10His tag can also be a potential binding site for ^{99m}Tc (*30*), which can be used for future SPECT imaging.

To the best of our knowledge, imaging of c-Met with rh-HGF has not been reported to date. In this study, we successfully developed and characterized ^{64}Cu-NOTA-rh-HGF for PET imaging of tumor c-Met expression in vivo. c-Met specificity of ^{64}Cu-NOTA-rh-HGF was demonstrated by several control experiments in vitro, in vivo, and ex vivo, making it a promising PET tracer with broad potential applications in the clinical diagnosis and treatment monitoring of cancer. With a molecular weight of about 90 kDa, rh-HGF is significantly smaller than monoclonal antibodies (typically 150 kDa). Therefore, ^{64}Cu-NOTA-rh-HGF cleared more quickly from the circulation than radiolabeled intact monoclonal antibodies. When compared with ^{89}Zr-labeled onartuzumab (a c-Met–targeting humanized 1-armed mAb with a similar molecular weight of ~99 kDa and a tumor-to-muscle ratio of 7.0 in U87MG tumor at 120 h after injection (*12*)), ^{64}Cu-NOTA-rh-HGF uptake in the U87MG tumor was much faster, with a significantly higher tumor-to-muscle ratio (13.5 ± 6.1 at 9 h after injection [$n = 4$]).

HGF contains 2 c-Met binding sites, including a high-affinity constitutively active site on the α chain and a low-affinity site on the β chain (*31*). Although the α chain of HGF activates c-Met and induces its dimerization, β-chain residues bind c-Met when the receptor binding site is located on the α chain and subsequently induce phosphorylation and downstream signaling (*31*). Our future work will focus on the design and purification of the α chain of rh-HGF with other labeling strategies, such as the use of shorter-lived PET isotopes with higher positron branching ratios (e.g., ^{61}Cu and ^{44}Sc) and testing of the resulting PET tracers in different tumor models. We believe that, on future clinical translation, noninvasive PET imaging with radiolabeled rh-HGF may support the selection of patients for c-Met–targeting drugs and identify responding and nonresponding patients for such therapeutics.

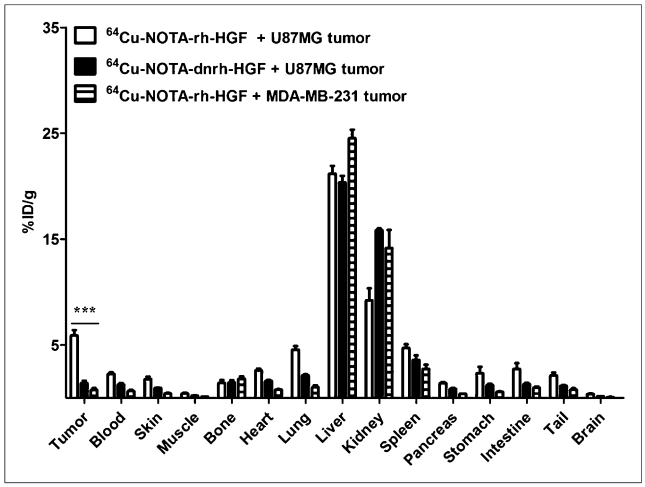

FIGURE 5. Biodistribution of ^{64}Cu-NOTA-rh-HGF in U87MG and MDA-MB-231 tumors, as well as ^{64}Cu-NOTA-dnrh-HGF in U87MG tumors, at 24 h after injection ($n \geq 3$).

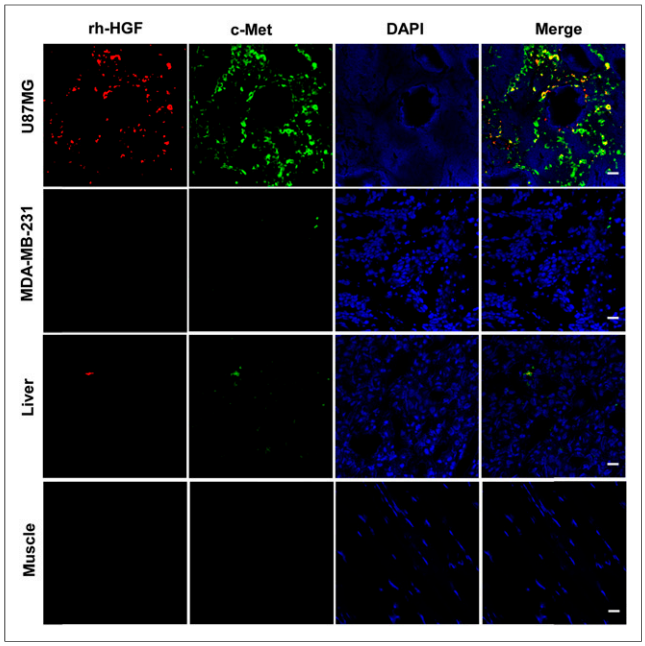

FIGURE 6. Immunofluorescence rh-HGF/c-Met/(4′,6-diamidino-2-phenylindole [DAPI]) triple staining of U87MG and MDA-MB-231 tumors, liver, and muscle tissue sections. Tissues were incubated with rh-HGF first, and mouse antihuman HGF antibody and FITC-conjugated goat antimouse IgG were used for rh-HGF staining (red). Rat antihuman c-Met antibody and Cy3-labeled donkey antirat IgG were used for c-Met staining (green). DAPI staining was used to reveal location of cell nuclei. Scale bar = 20 μm.

CONCLUSION

Herein we have reported the purification of rh-HGF, its characterization, and an in vitro and in vivo investigation of ^{64}Cu-NOTA-rh-HGF for PET imaging of c-Met expression in tumor models. Fast, prominent, and c-Met–specific uptake of ^{64}Cu-NOTA-rh-HGF in U87MG tumor was observed and then further validated by various in vivo and ex vivo experiments. On further optimization and development, rh-HGF–based PET tracers may be translated into the clinic for cancer diagnosis and prognosis based on c-Met targeting.

DISCLOSURE

The costs of publication of this article were defrayed in part by the payment of page charges. Therefore, and solely to indicate this fact, this article is hereby marked "advertisement" in accordance with 18 USC section 1734. This work was supported, in part, by the University of Wisconsin–Madison, the National Institutes of Health (NIBIB/NCI 1R01CA169365, P30CA014520, and T32CA009206), the Department of Defense (W81XWH-11-1-0644 and W81XWH-11-1-0648), and the American Cancer Society (125246-RSG-13-099-01-CCE). No other potential conflict of interest relevant to this article was reported.

REFERENCES

1. Birchmeier C, Birchmeier W, Gherardi E, Vande Woude GF. Met, metastasis, motility and more. *Nat Rev Mol Cell Biol.* 2003;4:915–925.
2. Christensen JG, Burrows J, Salgia R. c-Met as a target for human cancer and characterization of inhibitors for therapeutic intervention. *Cancer Lett.* 2005; 225:1–26.
3. Peruzzi B, Bottaro DP. Targeting the c-Met signaling pathway in cancer. *Clin Cancer Res.* 2006;12:3657–3660.
4. Garcia S, Dales JP, Charafe-Jauffret E, et al. Poor prognosis in breast carcinomas correlates with increased expression of targetable CD146 and c-Met and with proteomic basal-like phenotype. *Hum Pathol.* 2007;38:830–841.
5. Cappuzzo F, Janne PA, Skokan M, et al. MET increased gene copy number and primary resistance to gefitinib therapy in non-small-cell lung cancer patients. *Ann Oncol.* 2009;20:298–304.
6. Sattler M, Salgia R. c-Met and hepatocyte growth factor: potential as novel targets in cancer therapy. *Curr Oncol Rep.* 2007;9:102–108.
7. Ha SY, Lee J, Kang SY, et al. MET overexpression assessed by new interpretation method predicts gene amplification and poor survival in advanced gastric carcinomas. *Mod Pathol.* 2013;26:1632–1641.
8. Liu X, Newton RC, Scherle PA. Developing c-MET pathway inhibitors for cancer therapy: progress and challenges. *Trends Mol Med.* 2010;16:37–45.
9. You WK, McDonald DM. The hepatocyte growth factor/c-Met signaling pathway as a therapeutic target to inhibit angiogenesis. *BMB Rep.* 2008;41:833–839.
10. Terwisscha van Scheltinga AG, Lub-de Hooge MN, Hinner MJ, et al. In vivo visualization of MET tumor expression and anticalin biodistribution with the MET-specific anticalin ^{89}Zr-PRS-110 PET tracer. *J Nucl Med.* 2014;55:665–671.
11. Perk LR, Stigter-van Walsum M, Visser GW, et al. Quantitative PET imaging of Met-expressing human cancer xenografts with ^{89}Zr-labelled monoclonal antibody DN30. *Eur J Nucl Med Mol Imaging.* 2008;35:1857–1867.
12. Jagoda EM, Lang L, Bhadrasetty V, et al. Immuno-PET of the hepatocyte growth factor receptor Met using the 1-armed antibody onartuzumab. *J Nucl Med.* 2012;53:1592–1600.
13. Wang X, Liu H, Zhang Z, et al. High-level expression and characterization of bioactive human truncated variant of hepatocyte growth factor in Escherichia coli. *World J Microbiol Biotechnol.* 2014;30:2851–2859.
14. Wang MY, Yang YH, Lee HS, Lai SY. Production of functional hepatocyte growth factor (HGF) in insect cells infected with an HGF-recombinant baculovirus in a serum-free medium. *Biotechnol Prog.* 2000;16:146–151.
15. Stahl SJ, Wingfield PT, Kaufman JD, et al. Functional and biophysical characterization of recombinant human hepatocyte growth factor isoforms produced in Escherichia coli. *Biochem J.* 1997;326:763–772.
16. Grabenhorst E, Schlenke P, Pohl S, Nimtz M, Conradt HS. Genetic engineering of recombinant glycoproteins and the glycosylation pathway in mammalian host cells. *Glycoconj J.* 1999;16:81–97.
17. Nakamura T, Nishizawa T, Hagiya M, et al. Molecular cloning and expression of human hepatocyte growth factor. *Nature.* 1989;342:440–443.
18. Runge DM, Bowen WC, Katyal S, Runge D, Suski V, Michalopoulos GK. Expression of the human hepatocyte growth factor cDNA in primary cultures of rat hepatocytes. *Biochem Biophys Res Commun.* 1999;257:199–205.
19. Park JS, Kim H, Park J, et al. Overproduction of recombinant human hepatocyte growth factor in Chinese hamster ovary cells. *Protein Expr Purif.* 2010;70:231–235.
20. Hong H, Zhang Y, Nayak TR, et al. Immuno-PET of tissue factor in pancreatic cancer. *J Nucl Med.* 2012;53:1748–1754.
21. Luo H, Yang J, Jin H, et al. Tetrameric far-red fluorescent protein as a scaffold to assemble an octavalent peptide nanoprobe for enhanced tumor targeting and intracellular uptake in vivo. *FASEB J.* 2011;25:1865–1873.
22. Blumenschein GR Jr, Mills GB, Gonzalez-Angulo AM. Targeting the hepatocyte growth factor-cMET axis in cancer therapy. *J Clin Oncol.* 2012;30:3287–3296.
23. Gherardi E, Birchmeier W, Birchmeier C, Vande Woude G. Targeting MET in cancer: rationale and progress. *Nat Rev Cancer.* 2012;12:89–103.
24. Cullinane C, Dorow DS, Jackson S, et al. Differential ^{18}F-FDG and 3′-deoxy-3′-^{18}F-fluorothymidine PET responses to pharmacologic inhibition of the c-MET receptor in preclinical tumor models. *J Nucl Med.* 2011;52:1261–1267.
25. Wiehr S, von Ahsen O, Rose L, et al. Preclinical evaluation of a novel c-Met inhibitor in a gastric cancer xenograft model using small animal PET. *Mol Imaging Biol.* 2013;15:203–211.
26. Towner RA, Smith N, Doblas S, et al. In vivo detection of c-Met expression in a rat C6 glioma model. *J Cell Mol Med.* 2008;12:174–186.
27. Hurle RA, Davies G, Parr C, et al. Hepatocyte growth factor/scatter factor and prostate cancer: a review. *Histol Histopathol.* 2005;20:1339–1349.
28. Ido A, Moriuchi A, Marusawa H, et al. Translational research on HGF: a phase I/II study of recombinant human HGF for the treatment of fulminant hepatic failure. *Hepatol Res.* 2008;38(suppl 1):S88–S92.
29. Jäger V, Bussow K, Wagner A, et al. High level transient production of recombinant antibodies and antibody fusion proteins in HEK293 cells. *BMC Biotechnol.* 2013;13:52.
30. Waibel R, Alberto R, Willuda J, et al. Stable one-step technetium-99m labeling of His-tagged recombinant proteins with a novel Tc(I)-carbonyl complex. *Nat Biotechnol.* 1999;17:897–901.
31. Venepalli NK, Goff L. Targeting the HGF-cMET axis in hepatocellular carcinoma. *Int J Hepatol.* 2013:341636.